

# RoMA: Scaling up Mamba-based Foundation Models for Remote Sensing

Fengxiang Wang<sup>1</sup>, Hongzhen Wang<sup>2\*</sup>, Yulin Wang<sup>2</sup>, Di Wang<sup>3</sup>, Mingshuo Chen<sup>4</sup>,  
 Haiyan Zhao<sup>2</sup>, Yangang Sun<sup>2</sup>, Shuo Wang<sup>2</sup>, Long Lan<sup>1</sup>, Wenjing Yang<sup>1\*</sup>, Jing Zhang<sup>3\*</sup>  
<sup>1</sup> National University of Defense Technology, China <sup>2</sup> Tsinghua University, China  
<sup>3</sup> Wuhan University, China <sup>4</sup> Beijing University of Posts and Telecommunications, China

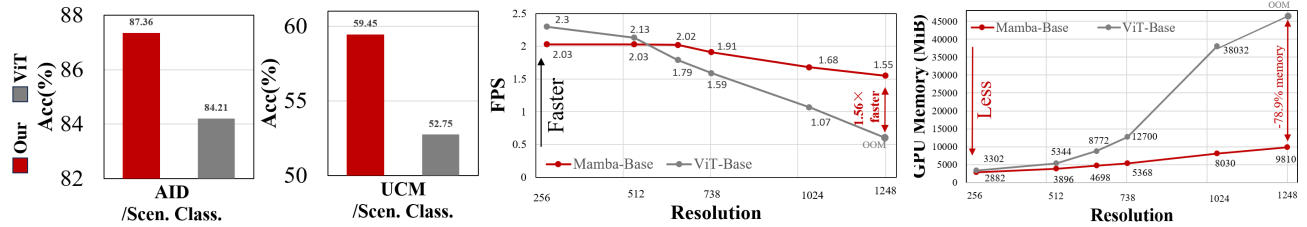


Figure 1. Comparison of ViT [13] (pretrained with MAE [17]) and our Mamba model (pretrained with RoMA) in scene classification, change detection, and semantic segmentation. Mamba outperforms ViT while being more computationally and memory efficient for high-resolution images. Notably, Mamba-B achieves 1.56× faster inference and reduces GPU memory usage by 78.9% on 1248×1248 resolution images (6084 tokens per image) on a single NVIDIA 4090PLUS GPU (batch size = 2).

## Abstract

Recent advances in self-supervised learning for Vision Transformers (ViTs) have fueled breakthroughs in remote sensing (RS) foundation models. However, the quadratic complexity of self-attention poses a significant barrier to scalability, particularly for large models and high-resolution images. While the linear-complexity Mamba architecture offers a promising alternative, existing RS applications of Mamba remain limited to supervised tasks on small, domain-specific datasets. To address these challenges, we propose RoMA, a framework that enables scalable self-supervised pretraining of Mamba-based RS foundation models using large-scale, diverse, unlabeled data. RoMA enhances scalability for high-resolution images through a tailored autoregressive learning strategy, incorporating two key innovations: 1) a rotation-aware pretraining mechanism combining adaptive cropping with angular embeddings to handle sparsely distributed objects with arbitrary orientations, and 2) multi-scale token prediction objectives that address the extreme variations in object scales inherent to RS imagery. Systematic empirical studies validate that Mamba adheres to RS data and parameter scaling laws, with performance scaling reliably as model and data size increase. Furthermore, experiments across scene classification, object detection, and semantic segmentation tasks demonstrate that

RoMA-pretrained Mamba models consistently outperform ViT-based counterparts in both accuracy and computational efficiency. The source code and pretrained models will be released at [RoMA](#).

## 1. Introduction

Over the past decade, advancements in remote sensing (RS) technology and more efficient data acquisition have significantly enhanced applications in ecosystem monitoring [42], and natural disaster management [3]. These applications rely on crucial model capabilities such as scene classification [21], object detection [24], change detection [58], and semantic segmentation [64]. However, training solely on limited task-specific data restricts the scale and generalizability of current RS deep learning models.

Recent breakthroughs in self-supervised learning (SSL) [17, 61] have led to the development of RS foundation models (RSFMs) [10, 23, 41, 44, 49, 53, 56, 62] that offer robust feature representations and excel across various remote sensing tasks. However, many of these tasks involve high-resolution imagery—such as the 4,000×4,000 pixel images in the DOTA dataset for object detection. Most RSFMs rely on Vision Transformer (ViT)-based attention architectures, whose quadratic complexity limits their practicality on high-resolution data. To overcome this challenge, researchers are exploring pretraining RSFMs on architec-

\*Corresponding authors

tures with linear complexity, with Mamba [68] emerging as a promising alternative.

The Mamba architecture is well-regarded in remote sensing for its efficient inference with high-resolution images in downstream tasks [6, 63]. However, current Mamba-based studies are limited to small-scale training datasets, restricting their exposure to diverse remote sensing data. This contrasts with trends in ViT-based RSFMs, which use self-supervised pretraining to harness extensive unlabeled data. Therefore, exploring self-supervised learning for Mamba to harness large-scale remote sensing data—and thereby compete with ViT—presents a promising, yet underexplored, direction.

Autoregressive pretraining [9, 50] offers a principled solution to Mamba’s sequence continuity challenges by representing images as 1-D sequences and employing next-token prediction. Its causal token dependencies naturally align with Mamba’s unidirectional linear-time scanning, preserving spatial coherence without the disruptions introduced by masking. While this approach has been successfully applied to natural images [9, 45, 50], RS images present unique challenges that remain largely unaddressed. We highlight three key challenges: (1) RS images often contain sparsely distributed foreground objects amid complex backgrounds. (2) Unlike objects in natural images, which typically maintain fixed orientations due to gravity, overhead RS images feature objects at varying orientations. (3) The wide range of object sizes in RS images complicates the extraction of effective representations. These challenges naturally lead to the question of whether Mamba-based RSFMs can scale efficiently with both increasing model size and larger data volumes—mirroring the performance improvements observed in self-supervised pretrained ViT architectures [34, 47].

To address these challenges, we propose Rotation-aware Multi-scale Autoregressive learning (RoMA), a framework that enables scalable self-supervised pretraining of Mamba-based RSFMs using large-scale, diverse, unlabeled data. Specifically, RoMA enhances scalability for high-resolution images through a tailored autoregressive learning strategy, incorporating two key innovations: (1) a rotation-aware pretraining mechanism combining adaptive cropping with angular embeddings to handle sparsely distributed objects with arbitrary orientations. By identifying key regions for rotation augmentation, it enhances rotation-invariant representation learning. Additionally, it embeds angle information during rotated cropping and requires the model to predict angular changes during autoregressive pretraining, further reinforcing rotation-invariant visual representations; and (2) multi-scale token prediction objectives that address the extreme variations in object scales inherent to RS imagery. By aggregating predicted token information across multiple spatial scales, this strategy helps Mamba capture more complete and structurally robust object representations during autoregressive pretraining.

Building on RoMA, we investigate its potential for pre-training Mamba-based RSFMs. Through systematic empirical studies, we confirm that Mamba aligns with RS data and parameter scaling laws, exhibiting reliable performance improvements as model and data size increase. Additionally, experiments across scene classification, object detection, and semantic segmentation tasks show that RoMA-pretrained Mamba models consistently surpass its ViT-based counterparts in both accuracy and computational efficiency.

The contributions of this study are as follows:

1. We introduce RoMA, the first self-supervised autoregressive pretraining framework for Mamba architectures in remote sensing, enabling efficient scaling to high-resolution RS imagery. RoMA validates that Mamba-based RSFMs follow scaling laws, achieving consistent performance gains with larger models and datasets.
2. We propose a dynamic rotation-aware mechanism that integrates adaptive region cropping and angle-aware embeddings. By guiding the model to predict angular variations during autoregressive learning, it effectively addresses rotational diversity and sparse target distributions, enhancing rotation-invariant feature learning.
3. We design a multi-scale prediction objective that addresses the extreme variations in object scales, enabling the model to learn robust object representations for downstream tasks.

## 2. Related Work

### 2.1. Remote Sensing Foundation Models

While vast amounts of RS data exist, much of it remains unlabeled and thus inaccessible for supervised learning [52]. Recently, self-supervised learning frameworks have been employed to learn representations from unlabeled RS data for tasks such as scene classification, object detection, and semantic segmentation. Self-supervised methods in RS mainly fall into two categories: generation-based methods [17] and contrastive learning-based methods [4]. As contrastive learning-based methods, GASSL [1] and CACo [35] use additional spatio-temporal information, while SeCo [36] focus on multiple Earth locations at different timestamps. Most recent work in RS has focused on generation-based self-supervised methods, like Masked Image Modeling (MIM) method, which can be further categorized as follows: leveraging general image knowledge [38], expanding parameter scales [5], integrating spatio-temporal information [10], addressing multi-sensor data [15, 19, 25, 40], and utilizing multi-scale concepts [41, 44, 49]. ScaleMAE [44], Cross-ScaleMAE [49], and SatMAE++ [41] use multi-scale concepts to enhance the performance with MIM method. MA3E [26] integrates remote sensing angle factors into the MIM training architecture for both the encoder and decoder.

While these methods have improved performance, they

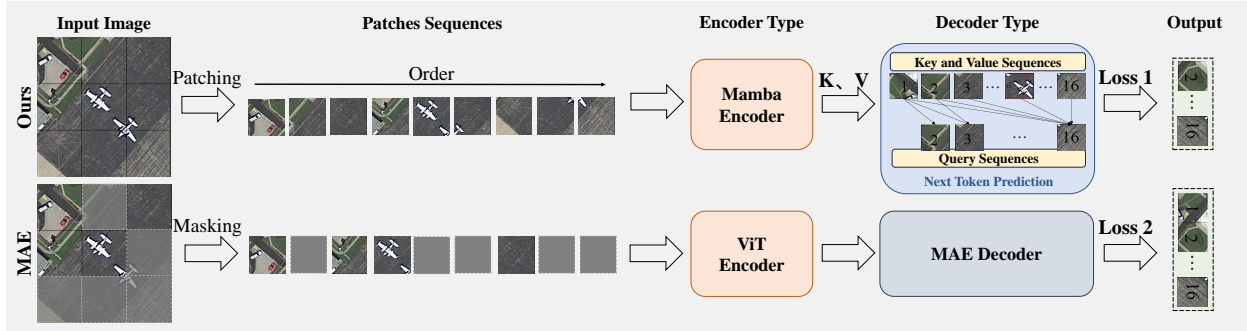


Figure 2. **The different between our autoregressive pretraining method and the MAE method.** Key differences: (1) Autoregressive pretraining encodes all image patches for the Mamba encoder, while MAE pretraining encodes only a randomly selected subset for the ViT encoder. (2) Autoregressive pretraining learns token sequence continuity through next-token prediction, whereas MAE reconstructs and predicts only randomly masked patches to compute the loss.

mainly concentrate on the ViT-based RSFMs and the MIM-based pretraining method. The Mamba-based RSFMs pretraining with the autoregressive method have not yet been explored by the RS community.

## 2.2. Vision Mamba in Remote Sensing

Recently, the Mamba architecture has excelled in NLP and has been adapted to the vision domain to address visual problems. Vision Mamba (Vim) [68] uses Vim blocks, consisting entirely of Mamba layers, with forward and backward scanning to model bidirectional representations. Vmamba [31] incorporates Visual State Space (VSS) blocks, combining Mamba and 2D convolution layers, supported by a Swin Transformer [32]-like pyramid architecture. The vision Mamba architecture has also expanded into remote sensing, producing various Mamba-based projects, categorized into four types: classification, detection, segmentation, and others. For classification, SSMamba [22] and SpectralMamba [63] handle hyperspectral data, while RSMamba [8] focuses on visible light. Detection methods like ChangeMamba [6] and RSCaMa [27] focus on change detection. Segmentation methods include Samba [69] and RS-Mamba [66], which use Mamba alone. Despite the growing research in RS using Mamba, current work is limited to supervised training on small-scale datasets, not fully exploiting the vast RS data.

## 2.3. Self-Supervised Learning in Vision

Inspired by the success of self-supervised learning in NLP, visual self-supervised learning methods are thriving in three main categories: contrastive learning [4, 16, 55], autoregressive learning [9, 14, 43], and Masked Image Modeling (MIM) [17, 61]. Current research on MIM focuses on regression targets and masking strategies. Various targets include discrete tokens [2], HOG features [57], deep features [67], and frequencies [28], have already been explored. However, MIM methods often face training issues while pretraining the Mamba architecture [45].

Recently, autoregressive pretraining in the visual domain has been explored. Most works, like VAR [50], have explored the application of autoregression in image generation. We are more focused on the work of autoregression in self-supervised pretraining. iGPT [9] first highlighted the potential of autoregressive pretraining as a general self-supervised visual representation strategy. SAIM [43], RandSAC [20] and AIM [14] explored further. These works mainly focus on pretraining the ViT series and have not explored pretraining the Mamba series. MAP [30] pretrained a hybrid Mamba-Transformer vision backbone network firstly. ARM [45] explored the compatibility of autoregressive pretraining with Mamba on the ImageNet [12] dataset, but it has not considered the specific issues of the RS field, like the rotation-invariant representations and various sizes information in RS images. Notably, while ARM has explored models of different sizes on natural images, it has not evaluated Mamba’s autoregressive pretraining performance across varying data scales. In the RS field, we are the first to establish the relationships between Mamba’s pretraining performance with data volume, and model size .

## 3. Method

### 3.1. Preliminaries

#### 3.1.1. Autoregressive Model

Considering a sequence of discrete tokens  $x = (x_1, x_2, \dots, x_N)$ , where  $x_n \in [S]$  is an integer from a vocabulary of size  $S$ . The next-token autoregressive model posits that the probability of observing the current token  $x_n$  depends only on its preceding tokens  $(x_1, x_2, \dots, x_{n-1})$ . This unidirectional token dependency assumption enables the factorization of the sequence  $x$ ’s likelihood as follows:

$$p(x_1, x_2, \dots, x_N) = \prod_{n=1}^N p(x_n | x_1, x_2, \dots, x_{n-1}) \quad (1)$$

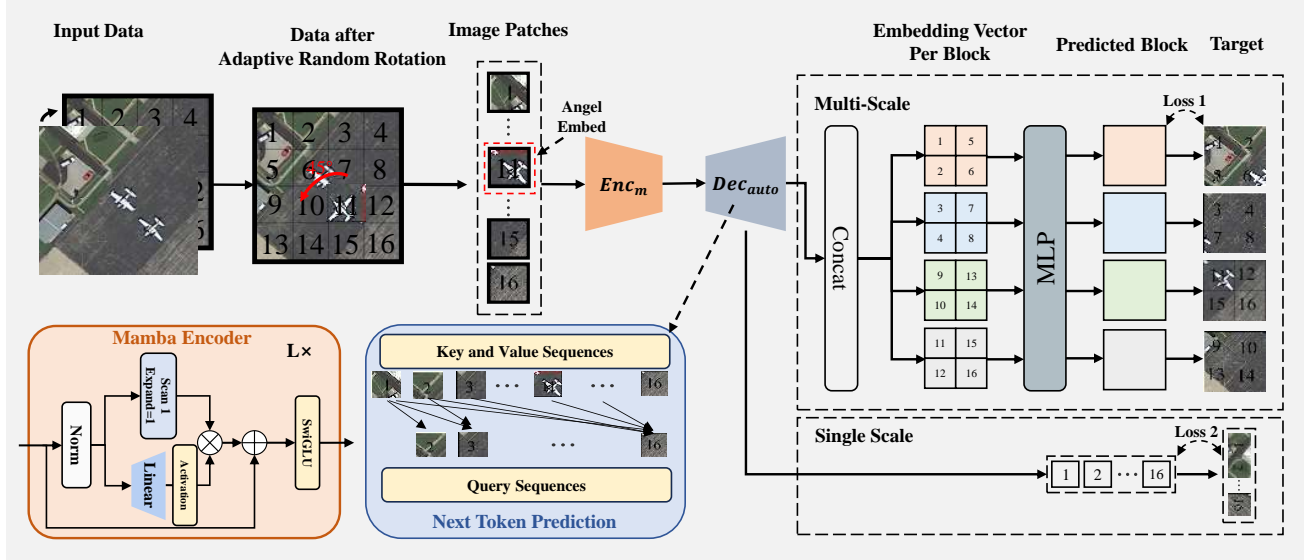


Figure 3. **Overview of the RoMA Pretraining Pipeline.** The input image is first divided into patches, and high-value patches are selected for random rotation using the Adaptive Rotation Encoding Strategy. These patches are then tokenized and processed by the Mamba encoder. The encoded features undergo autoregressive next-token prediction, followed by a multi-scale strategy that computes losses at different scales for gradient updates. RoMA optimally adapts the Mamba architecture for remote sensing, making its encoder a robust feature extractor for diverse downstream tasks.

Training an autoregressive model  $p_\phi$  involves optimizing  $p_\phi(x_n | x_1, x_2, \dots, x_{n-1})$  over a dataset. This process, known as the next-token prediction, allows the trained  $p_\phi$  to generate new sequences.

### 3.1.2. Autoregressive Pretraining of Mamba

Previous work [10, 41, 44, 53, 56] primarily used MAE-based methods for pretraining RSFMs. However, these are mainly applicable to ViT-based RSFMs. As discussed in Section 1, high-resolution remote sensing scenarios demand RSFMs with linear complexity, not the quadratic complexity of ViT series models. Therefore, as shown in Figure 1, we compared the accuracy, speed, and GPU memory usage of our Mamba architecture with the typical ViT model at various resolutions. The results clearly show that Mamba, with its linear complexity, outperforms ViT-based models in high-resolution scenarios.

Moreover, MAE-based methods in previous works are ineffective for pretraining Mamba-based RSFMs. We identify two reasons for using autoregressive pretraining with a Mamba architecture in RS: 1) the advantage of autoregression due to its encoding similarity to Mamba, and 2) the drawback of MAE, which disrupts token sequences.

**A autoregressive Advantage:** Both autoregressive models and Mamba perform patch-based operations (e.g., Mamba scans a single patch) and process sequences in order. As shown in Figure 2, autoregressive modeling constructs all patches sequentially, predicting the next token within the sequence. Similarly, Mamba’s core Scan Blocks process the

entire image in order. This consistent encoding makes autoregressive pretraining a better fit for Mamba architecture.

**MAE’s Disruption of Token Sequence:** Unlike autoregressive encoding, MAE masks part of the tokens and learns by reconstructing the masked ones. Masking, a key operation of MAE, disrupts the relationships between sequential tokens. As illustrated in Figure 2, after masking, MAE retains only a subset of unconnected tokens, preventing Mamba-based encoders from performing linear scanning. Mamba’s linear scan processes temporally related tokens, not randomly related ones.

Given the advantages of autoregressive methods and the disruptive nature of MAE, we favor autoregressive methods for pretraining Mamba. Expanding on the theoretical analysis, the experiments which comparing MAE and Mamba [45] on various downstream tasks highlight the strong compatibility of autoregressive architectures with Mamba. In remote sensing field, consistent with ARM [45]’s conclusions in the natural image domain. We hope this establishes autoregressive architectures as a solid baseline for Mamba pretraining in remote sensing and inspires further research.

### 3.2. RoMA

We propose the RoMA autoregressive pretraining framework for the Mamba architecture in RS field. Specially, as shown in the Figure 3, we extend the iGPT [9] series with a  $KV$  cache-based prediction method. The Mamba-Encoder processes the entire image to compute the  $Key$  and  $Value$  for

all tokens. Then we calculate the learnable query vector from the *Key* and *Value*, and compute the loss between the *Query* and the target ground truth. Building on the autoregressive pretraining structure for natural images, RoMA introduces two key contributions: an adaptive rotation encoding strategy and a multi-scale prediction strategy.

### 3.2.1. Adaptive Rotation Encoding Strategy

Autoregressive pretraining for natural images does not consider the uneven, sparse information distribution and rotational invariance in RS images. For instance, as shown in Figure 4, RS images contain redundant airport runway pixels, and varying airplane angles lead to different postures and shapes. These unique characteristics prompt us to rethink how the encoder can learn high knowledge density features with rotational invariance. In RoMA, we propose an adaptive rotation encoding strategy to enhance autoregressive pretraining for remote sensing.

Given an input image  $x \in \mathbb{R}^{H \times W \times C}$ , it is reshaped into  $N = (H \times W)/p^2$  non-overlapping patches  $x^p \in \mathbb{R}^{N \times (p^2 C)}$ , where  $p$  is the patch size,  $(H, W)$  is the size of the input image, and  $C$  is the number of channels. We compute the features  $F(\cdot)$  of each patch using a traditional feature descriptor, like LBP [18] and select the token with the highest feature values. The process can be formulated as:

$$token_{top} = \{x_i^p | i = m, m \in top_K(F(\{x_i^p\}_{i=1}^N))\}, \quad (2)$$

where  $token_{top}$  denotes the selected token and  $top_K(\cdot)$  denotes the index set of the selected top tokens with number of  $K$ . Then, centered on the patch represented by  $token_{top}$ , we expand its size to obtain a larger, more suitable region. Specifically, we select all patches in the image that contain  $token_{top}$  with a fixed edge length of  $L_i$  pixels, as defined by the following formula:

$$token_{L_i} = \{x_{(i_h, i_w)}^p | i_h = [m - (L_i/p), m + (L_i/p)], \\ i_w = [m - (L_i/p), m + (L_i/p)], \mathcal{L}(i_w) = \mathcal{L}(i_h) = L_i/p\} \quad (3)$$

where  $(i_h, i_w)$  defines the horizontal and vertical range of selected tokens within the sequentially ordered tokens of the original image.  $\mathcal{L}$  represents the interval length, calculated based on patch size. After extracting a square token region  $token_{L_i}$  with an edge length of  $L = \{96, 64, 32\}$ ,  $L_i \in L$ , we compute its average feature value and compare it with the average feature value of each patch in the original image. If  $token_{L_i}$  has a higher average feature value  $avg_{all} = Avg(F(\{x_i^p\}_{i=1}^N))$ , it is identified as a high-value region and proceeds to the rotation step. Otherwise, a smaller  $L_i$  is selected, and Eq. 3 is reapplied. This process repeats up to three times until a region with a higher average feature

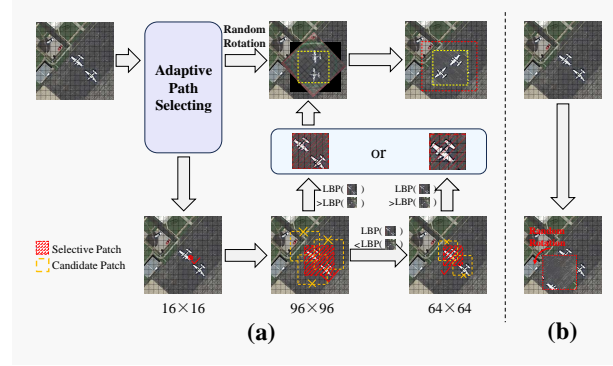


Figure 4. **Illustration of the Adaptive Rotation Encoding Strategy.** (a) Pipeline of the Adaptive Rotation Encoding Strategy. (b) Random patch selection for rotation without adaptive selection. The random approach in (b) disrupts object information in the RS image.

value than the original image is found. The corresponding formula is as follows:

$$token_L = \begin{cases} token_{L_i}, & Avg(F(token_{L_i})) \geq avg_{all} \\ token_{L_{i+1}}, & Avg(F(token_{L_{i+1}})) \geq avg_{all} \\ token_{L_{i+2}}, & \text{otherwise} \end{cases} \quad (4)$$

The selected  $token_L$  is cropped to generate diverse rotated remote sensing scenes. For a square region  $token_L$  with edge length  $L$ , random rotation may cause edge information loss. To mitigate this, we follow MA3E [26] and apply center cropping to retain the inscribed square (marked in yellow) within the largest inscribed circle. This region, oriented in any direction, replaces the original scene and introduces explicit angular variations. In addition to positional embeddings, we incorporate learnable angle embeddings shared across patches within the rotated crop. These serve as implicit cues, helping the model perceive angular changes while distinguishing them from the background.

Finally, the Adaptive Rotation Encoding Strategy processes the image before feeding it into the Mamba-based encoder for representation learning. RoMA follows the standard Mamba architecture [45] without modifications, focusing purely on pretraining Mamba for RS field. While architectural improvements could enhance performance and efficiency, RoMA prioritizes pretraining strategies, leaving further Mamba optimizations to future research.

### 3.2.2. Multi-scale Prediction Strategy

Images are continuous 2D signals. To apply autoregressive pretraining via next-token prediction, two steps are required: (1) Convert images into discrete tokens. (2) Define them as a one-dimensional sequence for unidirectional modeling. Methods like iGPT [9] and VAR [50] tackle these challenges by slicing images into segments and arranging them into a feature sequence in a specified one-dimensional order.

However, as discussed in Section 1, directly applying this method to RS images fails to consider key factors. Unlike natural images, which focus on visual semantic understanding, RS images focus on surface measurement information [65]. Arbitrarily

Table 1. The configuration of different architecture variants.

Model	Block	Width	Depth	Param.(M)
ViT-T	Attention+MLP	192	12	5.7
Mamba-T	Mamba+MLP	192	12	5.3
ViT-S	Attention+MLP	384	12	22
Mamba-S	Mamba+MLP	384	12	21
ViT-B	Attention+MLP	768	12	86
Mamba-B	Mamba+MLP	768	12	85
ViT-L	Attention+MLP	1024	24	307
Mamba-L	Mamba+MLP	1024	24	297

disrupting spatial relationships in RS images leads to fundamentally different interpretations. For example, token  $x^{(i,j)}$  and its neighbors  $x^{(i\pm 1,j)}$ ,  $x^{(i,j\pm 1)}$  are closely related due to planar surface measurements. As seen in Figure 2, the token  $x^{(i,j)}$  representing the part of plane is closely related to vertical neighboring tokens and some distant vertical tokens. The unidirectional flattening of autoregressive methods compromises surface information representation in RS images. Therefore, we introduce a multi-scale prediction strategy to mitigate the effects of unidirectional flattening.

The Mamba-based encoder generates *key* and *value* feature representations for each token. During decoding, we apply cross-attention with token-level causal masking to sequentially predict tokens, ensuring each token relies only on previously observed ones. The decoder performs autoregressive prediction at the token level. Once the decoder produces predictions, the autoregressive process compares them with their corresponding tokens in the original image for learning. Mean squared error (MSE) is used as the loss function.

Building on MSE loss function, we concatenate token representations from each decoder block at a higher scale following a predefined raster order. A fully connected multi-layer perceptron (MLP) then reconstructs the pixel values of the next block. Notably,  $x_k \in \mathcal{R}^{16 \times 16}$ , while at a higher scale, spatial aggregation results in  $y_n \in \mathcal{R}^{s \times s}$ .  $s$  is the pixel size value of larger scale. The formula is as follows:

$$\ell(\theta) = \frac{1}{K-1} \sum_{k=2}^K \|\hat{x}_k(\theta; x_{<k}) - x_k\|_2^2 + \frac{\lambda}{N-1} \sum_{n=2}^N \|\hat{y}_n(\theta; y_{<n}) - y_n\|_2^2 \quad (5)$$

where  $\theta$  represents the network parameters,  $N$  is the number of cluster blocks in an image,  $y_n$  is the ground truth pixel value of the  $n$ -th cluster block, and  $\hat{y}_n(\theta; y_{<n})$  denotes the reconstructed value based on  $\theta$  and preceding tokens ( $y_{<n}$ ),  $K$  is the number of all tokens in an image,  $x_k$  denotes the ground truth pixel value of the  $k$ -th token, and  $\hat{x}_k(\theta; x_{<k})$  is the reconstructed value based on the network parameters ( $\theta$ ) and preceding tokens ( $x_{<k}$ ) in the sequence. The parameter  $\lambda$  regulates the contribution of the MSE loss from higher-scale cluster blocks to the overall loss.

### 3.3. Scaling Mamba-based RSFMs

To investigate the scaling potential of the self-supervised pretrained Mamba architecture for developing powerful RSFMs. With RoMA,

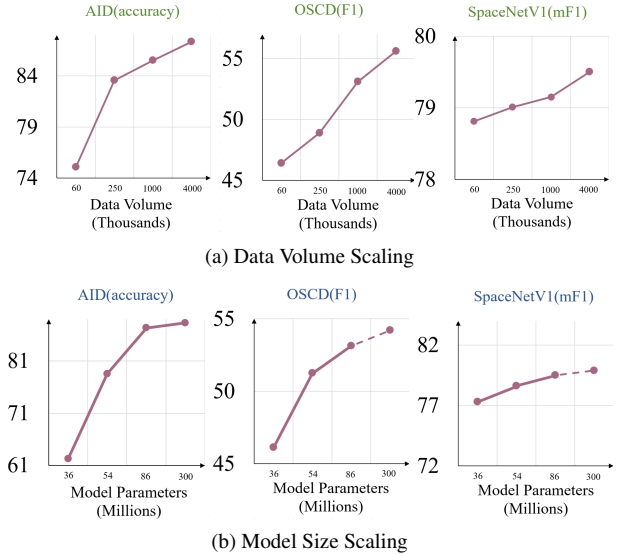


Figure 5. **Scaling with Data Volume and Model Size.** (a) We showcase the Mamba-Base model’s performance on three downstream tasks after RoMA pretraining with different data scales. (b) We compare the performance of various Mamba model sizes on three downstream tasks, all pretrained with 4 million data using RoMA. Details on pretraining and downstream task configurations are provided in Section 4.1.

we analyze the relationships between Mamba’s performance with model parameters, and data scale.

The scalability of ViT architectures pretrained with MAE has been well established, demonstrating performance gains with increasing data volume and model size [34, 47]. However, no prior work has systematically examined whether the Mamba architecture follows a similar trend in RS field. For the first time, we explore Mamba’s scaling behavior in RS domain using the RoMA pretraining method.

**Scaling with Data Volume:** Mamba shows a clear performance boost on downstream tasks as the pretraining data volume grows. We pretrain the Mamba-Base model with RoMA across various data scales and evaluate its performance in the downstream tasks. As illustrated in Figure 5a, larger datasets lead to significant improvements. Mamba-based RSFMs exhibit no significant performance bottlenecks across a broad pretraining data scale from 62.5K to 4M, achieving data learning capabilities on par with ViT-based RSFMs. We look forward to future advancements of data volume in remote sensing, where larger datasets can further enhance Mamba-based RSFMs through our RoMA pretraining framework.

**Scaling with Model Size:** Mamba’s performance also improves with increasing model size. We conduct extensive pretraining on four model variants—Tiny, Small, Base, and Large—following the configurations in our code. As shown in Figure 5b, larger models consistently achieve superior results on downstream tasks. Although Mamba-Large surpasses Mamba-Base in AID dataset, its performance gain remains limited, likely due to insufficient pretraining. With only 300 epochs on 4 million samples, the training may not be adequate for a 297M-parameter model. Due to exper-

Table 2. Results for scene classification, change detection, and semantic segmentation. “TR” represents the ratio of training data. \* indicates results from MA3E [26] and MTP [54]. † denotes our reproduction with their official code.

Methods	Publication	Backbone	Params	Scene Classification		Change Detection	Semantic Segmentation
				AID	UCM	OSCD	SpaceNetv1
				OA(TR=50%)	OA(TR=50%)	F1	mF1
<i>Natural Image pretraining</i>							
MoCo v3 * [16]	ICCV’21	ViT-B	86M	78.72	38.34	-	-
DINO * [4]	ICCV’21	ViT-B	86M	78.51	40.04	-	-
MAE * [17]	CVPR’22	ViT-B	86M	84.21	52.75	-	-
SimMIM * [61]	CVPR’22	ViT-B	86M	83.19	51.48	-	-
LoMaR * [7]	Arxiv’22	ViT-B	86M	82.26	51.89	-	-
MixMAE * [29]	CVPR’23	Swin-B/W14	88M	81.53	50.63	-	-
ARM †[45]	ICLR’25	Mamba-B	85M	81.14	50.41	47.28	77.89
<i>RS Image pretraining</i>							
SeCo * [36]	ICCV’21	ResNet-50	25.6M	78.26	47.45	47.67	77.09
CACo * [35]	CVPR’23	ResNet-50	25.6M	77.81	40.53	52.11	77.94
SatMAE * [10]	NIPS’22	ViT-L	307M	55.10	34.28	52.76	78.07
ScaleMAE * [44]	ICCV’23	ViT-L	307M	48.46	28.19	-	-
GFM * [38]	ICCV’23	Swin-B	88M	80.58	49.73	-	-
RVSA * [53]	TGRS’23	ViT-B+RVSA	86M	84.06	50.86	50.28	<b>79.56</b>
SatMAE++ † [41]	CVPR’24	ViT-L	307M	85.98	55.72	53.10	79.21
MA3E * [26]	ECCV’24	ViT-B	86M	85.86	55.69	-	-
RoMA	-	Mamba-B	85M	<b>87.36</b>	<b>59.45</b>	<b>55.63</b>	79.50

imental constraints, we did not extend pretraining to 800 epochs as in MAE. The OSCD and SpaceNet experiments are ongoing, with updates to follow. However, these results do not alter our key findings: Mamba-based RSFMs pretrained with RoMA demonstrate performance gains as model parameters scale. While this growth remains inconclusive in more large-scale experiments, we anticipate future research will further explore Mamba’s scaling potential.

## 4. Experiments

We pretrain Mamba extensively using RoMA and assess its effectiveness across diverse downstream tasks. Finally, we conduct thorough ablation studies on RoMA’s design choices.

### 4.1. Pretraining and Downstream Tasks

**Pretraining Setup.** Our pretraining experiment setup largely follows ARM [45]. We train both the Mamba-B on the OpticalRS-4M [56]. We adjust the input image to a size of  $196 \times 196$ , with a patch size of 16, using the AdamW optimizer and a cosine learning rate scheduler. The initial learning rate is set to  $1.5e-4$ , and batch size is set to 256, with a epoch of 400.

**Downstream Tasks.** We further evaluated RoMA across three key downstream tasks: scene classification, change detection, and semantic segmentation. In addition to benchmarking against ViT-based RSFMs, like SatMAE[10], SatMAE++ [41], ScaleMAE[44], SeCo[36], CACo [35], RingMo[48], CMID[39], RVSA [53] and GFM[38], we compared RoMA with other pretraining methods for natural images. These encompass methods leveraging contrastive learning and generative learning, including MoCo v3 [16], DINO [4], MAE [17], SimMIM [61], LoMaR [7] and MixMAE [29], and

autogressive pretraining approaches, ARM [45]. The Mamba-B architectures strictly adhere to the simplest Mamba design from ARM, without any modifications, allowing us to exhaustively test the advantages of the RoMA pretraining framework.

**Scene Classification.** We first assess the pretrained model’s performance on the scene classification task using linear probing. By freezing the model’s parameters and fine-tuning only the final fully connected (FC) layer, linear probing effectively demonstrates its feature extraction ability. Since full-parameter fine-tuning already achieves over 99% performance on classification datasets, like AID [59], we prefer linear probing rather than fine tuning. We use two scene classification datasets: AID [59] and UCM [37], with training details, including the train-test split ratio, following [44, 53]. Evaluation is based on overall accuracy (OA). The results in Table 2 show RoMA’s competitive performance compared to other pretraining methods.

**Change Detection.** We used the OSCD [11] dataset consisting of RGB images for change detection. Following previous works [54], we kept the experimental setups consistent, using UNet [46] as the decoder. Detailed configurations are provided in the code, with results summarized in Table 2. On the OSCD dataset, our method outperforms ARM [45] and other methods that overlook rotational invariance and information sparsity and varying object size issues in RS.

**Semantic Segmentation.** We further evaluate the pretrained model on semantic segmentation tasks, using common remote sensing datasets: SpaceNetv1 [51]. Our implementation follows [54], using UperNet [60] as the segmentation framework. Table 2 highlights RoMA’s superiority over competitors in pixel-level scene parsing. However, in pixel-level tasks, Mamba-based RSFMs show

Table 3. Ablation study on the design choices of RoMA with Mamba-B backbone. We report the top-1 accuracy (%). The default settings of RoMA are highlighted in grey.

(a) <b>Main ablation.</b> Adaptive Rotation Encoding Strategy. Local Binary Pattern (LBP) measurement outperforms the Wavelet Transform and coding Strategy. Three layers is the most effective choice. (MSP) significantly improve RoMA.				(b) <b>Feature Descriptor</b> in Adaptive Rotation En-			(c) <b>Selecting Patch Size</b> in Adaptive Rotation En-		
ARE	MSP	AID		Feature Descriptor	AID		Patch Size	AID	
		OA (TR=20%)	OA (TR=50%)		OA (TR=20%)	OA (TR=50%)		OA (TR=20%)	OA (TR=50%)
		69.59	76.80	Wavelet	71.42	77.00	96	70.48	76.82
✓		71.70	78.00	HOG	71.94	78.32	96-32	71.23	77.12
✓	✓	72.69	79.16	LBP	71.70	78.00	96-64-32	71.70	78.00

(d) <b>Threshold</b> for patch selection in the Adaptive Rotation Encoding Strategy is based on the im-age’s overall average computed ( <i>Avg.</i> ) from the $\lambda$ in Equation 3 in Multi-scale Prediction Strategy. Feature Descriptor .				(e) <b>Coefficient <math>\lambda</math>.</b> The variation of the coefficient tion Strategy. Experiments were conducted using the standard 16×16 patch as a baseline, with additional combinations at multiples of 2-6.				
Threshold	AID		Coefficient $\lambda$	AID		Multi-scale Prediction Strategy	AID	
	OA (TR=20%)	OA (TR=50%)		OA (TR=20%)	OA (TR=50%)		OA (TR=20%)	OA (TR=50%)
1.5 × <i>Avg.</i>	68.33	72.39	0.01	71.81	78.23	2×+4×+6×	63.17	71.34
0.5 × <i>Avg.</i>	69.71	74.18	1.0	70.92	77.49	2×+4×	68.06	74.74
1.0 × <i>Avg.</i>	71.70	78.00	0.1	72.69	79.16	4×+6×	67.81	74.32
						4×	72.46	78.72
						6×	72.69	79.16

less pronounced advantages compared to other downstream tasks. We attribute this to RoSA’s autoregressive pretraining, which prioritizes multi-scale patch-based targets over pixel-level prediction. While this improves semantic understanding in classification and detection, a slight trade-off in pixel-level comprehension is expected.

## 4.2. Ablation Study

Due to resource constraints, we conducted the ablation experiments using the MillionAID [33] dataset and trained for 400 epochs. For downstream tasks, we present the linear probing results across two settings on AID datasets.

Table 3a presents the performance of RoMA’s two main contributions, with ARM as the baseline. The experiment shows a significant gain in feature extraction capability. Tables 3b and 3c adding the Adaptive Rotation Encoding Strategy on the baseline. Table 3b comparing the effects of different Feature Descriptors. We believe the Feature Descriptor method can be further optimized without affecting the Adaptive Rotation Encoding Strategy’s effectiveness. Table 3c evaluates patch sizes for rotation, showing that various sizes improve performance.

Tables 3d, 3e, and 3f examine the Multi-scale Prediction Strategy. The parameter and threshold selections are shown in Tables 3d and 3e, while Table 3f presents the performance of aggregating spatial features from multiple scales. Our results indicate that adding excessive multi-scale information doesn’t guarantee improved performance; instead, using only large-scale aggregated information along with the original 16×16 patch data yields better results.

## 5. Conclusion

We introduce RoMA, the first self-supervised autoregressive framework to scale Mamba-based foundation models for RS. RoMA addresses two key challenges: handling sparsely distributed objects with arbitrary orientations via dynamic angle-aware tokenization, and addressing extreme variations in object scales

through multi-scale token prediction. By leveraging large-scale, diverse, unlabeled data, RoMA enables scalable self-supervised pretraining of Mamba-based RS models. Extensive experiments across scene classification, object detection, and semantic segmentation show that RoMA-pretrained Mamba models consistently outperform ViT-based counterparts. Additionally, these models achieve significant efficiency improvements, reducing GPU memory consumption by 78.9% and accelerating inference speed by 1.56× at 1,248×1,248 resolution, while maintaining linear computational scaling. Our findings also provide new insights into Mamba’s scaling laws, demonstrating consistent performance gains with increasing data volume (6.25M → 400M) and model size (5.3M → 297M parameters), highlighting its potential for large-scale Earth observation tasks.

## References

- [1] Kumar Ayush, Burak Uzcent, Chenlin Meng, Kumar Tanmay, Marshall Burke, David Lobell, and Stefano Ermon. Geography-aware self-supervised learning. In *ICCV*, pages 10161–10170, 2021. 2
- [2] Hangbo Bao, Li Dong, Songhao Piao, and Furu Wei. Beit: Bert pre-training of image transformers. In *ICLR*, 2021. 3
- [3] Olalekan Mumin Bello and Yusuf Adedoyin Aina. Satellite remote sensing as a tool in disaster management and sustainable development: Towards a synergistic approach. *Procedia-Social and Behavioral Sciences*, 120:365–373, 2014. 1
- [4] Mathilde Caron, Hugo Touvron, Ishan Misra, Hervé Jégou, Julien Mairal, Piotr Bojanowski, and Armand Joulin. Emerging properties in self-supervised vision transformers. In *ICCV*, pages 9630–9640, 2021. 2, 3, 7
- [5] Keumgang Cha, Junghoon Seo, and Taekyung Lee. A billion-scale foundation model for remote sensing images. *IEEE Journal of Selected Topics in Applied Earth Observations and Remote Sensing*, pages 1–17, 2024. 2

- [6] Hongruixuan Chen, Jian Song, Chengxi Han, Junshi Xia, and Naoto Yokoya. Changemamba: Remote sensing change detection with spatiotemporal state space model. *IEEE Transactions on Geoscience and Remote Sensing*, 62:1–20, 2024. 2, 3
- [7] Jun Chen, Ming Hu, Boyang Li, and Mohamed Elhoseiny. Efficient self-supervised vision pretraining with local masked reconstruction. *arXiv preprint arXiv:2206.00790*, 2022. 7
- [8] Keyan Chen, Bowen Chen, Chenyang Liu, Wenyuan Li, Zhengxia Zou, and Zhenwei Shi. Rsmamba: Remote sensing image classification with state space model. *IEEE Geoscience and Remote Sensing Letters*, pages 1–5, 2024. 3
- [9] Mark Chen, Alec Radford, Rewon Child, Jeffrey Wu, Heewoo Jun, David Luan, and Ilya Sutskever. Generative pretraining from pixels. In *ICML*, pages 1691–1703. PMLR, 2020. 2, 3, 4, 5
- [10] Yezhen Cong, Samar Khanna, Chenlin Meng, Patrick Liu, Erik Rozi, Yutong He, Marshall Burke, David Lobell, and Stefano Ermon. Satmae: Pre-training transformers for temporal and multi-spectral satellite imagery. *Advances in Neural Information Processing Systems*, 35:197–211, 2022. 1, 2, 4, 7
- [11] Rodrigo Caye Daudt, Bertr Le Saux, Alexandre Boulch, and Yann Gousseau. Urban change detection for multispectral earth observation using convolutional neural networks. In *IGARSS 2018-2018 IEEE International Geoscience and Remote Sensing Symposium*, pages 2115–2118. IEEE, 2018. 7
- [12] Jia Deng, Wei Dong, Richard Socher, Li-Jia Li, Kai Li, and Li Fei-Fei. Imagenet: A large-scale hierarchical image database. In *CVPR*, pages 248–255. IEEE, 2009. 3
- [13] Alexey Dosovitskiy, Lucas Beyer, Alexander Kolesnikov, Dirk Weissenborn, Xiaohua Zhai, Thomas Unterthiner, Mostafa Dehghani, Matthias Minderer, Georg Heigold, Sylvain Gelly, Jakob Uszkoreit, and Neil Houlsby. An image is worth 16x16 words: Transformers for image recognition at scale. In *ICLR*, 2021. 1
- [14] Alaaeldin El-Nouby, Michal Klein, Shuangfei Zhai, Miguel Angel Bautista, Vaishaal Shankar, Alexander Toshev, Joshua M Susskind, and Armand Joulin. Scalable pre-training of large autoregressive image models. In *ICML*. JMLR.org, 2024. 3
- [15] Xin Guo, Jiangwei Lao, Bo Dang, Yingying Zhang, Lei Yu, Lixiang Ru, Liheng Zhong, Ziyuan Huang, Kang Wu, Dingxiang Hu, Huimei He, Jian Wang, Jingdong Chen, Ming Yang, Yongjun Zhang, and Yansheng Li. Skysense: A multi-modal remote sensing foundation model towards universal interpretation for earth observation imagery. In *CVPR*, pages 27672–27683, 2024. 2
- [16] Kaiming He, Haoqi Fan, Yuxin Wu, Saining Xie, and Ross B. Girshick. Momentum contrast for unsupervised visual representation learning. In *CVPR*, pages 9726–9735. Computer Vision Foundation / IEEE, 2020. 3, 7
- [17] Kaiming He, Xinlei Chen, Saining Xie, Yanghao Li, Piotr Dollár, and Ross B. Girshick. Masked autoencoders are scalable vision learners. In *CVPR*, pages 15979–15988. IEEE, 2022. 1, 2, 3, 7
- [18] Marko Heikkilä, Matti Pietikäinen, and Cordelia Schmid. Description of interest regions with local binary patterns. *Pattern recognition*, 42(3):425–436, 2009. 5
- [19] Danfeng Hong, Bing Zhang, Xuyang Li, Yuxuan Li, Chenyu Li, Jing Yao, Naoto Yokoya, Hao Li, Pedram Ghamisi, Xiuping Jia, Antonio Plaza, Paolo Gamba, Jón Atli Benediktsson, and Jocelyn Chanussot. Spectralgpt: Spectral remote sensing foundation model. *IEEE Trans. Pattern Anal. Mach. Intell.*, 46(8):5227–5244, 2024. 2
- [20] Tianyu Hua, Yonglong Tian, Sucheng Ren, Michalis Raptis, Hang Zhao, and Leonid Sigal. Self-supervision through random segments with autoregressive coding (randsac). In *ICLR*, 2022. 3
- [21] Liang Huang, Fengxiang Wang, Yalun Zhang, and Qingxia Xu. Fine-grained ship classification by combining cnn and swin transformer. *Remote Sensing*, 14(13):3087, 2022. 1
- [22] Lingbo Huang, Yushi Chen, and Xin He. Spectral-spatial mamba for hyperspectral image classification. *Remote Sensing*, 16(13), 2024. 3
- [23] Long Lan, Fengxiang Wang, Shuyan Li, Xiangtao Zheng, Zengmao Wang, and Xinwang Liu. Efficient prompt tuning of large vision-language model for fine-grained ship classification. *arXiv preprint arXiv:2403.08271*, 2024. 1
- [24] Wentong Li, Yijie Chen, Kaixuan Hu, and Jianke Zhu. Oriented reprints for aerial object detection. In *CVPR*, pages 1829–1838, 2022. 1
- [25] Xuyang Li, Danfeng Hong, and Jocelyn Chanussot. S2mae: A spatial-spectral pretraining foundation model for spectral remote sensing data. In *CVPR*, pages 24088–24097, 2024. 2
- [26] Zhihao Li, Biao Hou, Siteng Ma, Zitong Wu, Xianpeng Guo, Bo Ren, and Licheng Jiao. Masked angle-aware autoencoder for remote sensing images. In *ECCV*, pages 260–278. Springer, 2025. 2, 5, 7
- [27] Chenyang Liu, Keyan Chen, Bowen Chen, Haotian Zhang, Zhengxia Zou, and Zhenwei Shi. Rscama: Remote sensing image change captioning with state space model. *IEEE Geosci. Remote. Sens. Lett.*, 21:1–5, 2024. 3
- [28] Hao Liu, Xinghua Jiang, Xin Li, Antai Guo, Yiqing Hu, Deqiang Jiang, and Bo Ren. The devil is in the frequency: Geminated gestalt autoencoder for self-supervised visual pretraining. In *AAAI*, pages 1649–1656, 2023. 3
- [29] Jihao Liu, Xin Huang, Jinliang Zheng, Yu Liu, and Hongsheng Li. Mixmae: Mixed and masked autoencoder for efficient pretraining of hierarchical vision transformers. In *CVPR*, pages 6252–6261, 2023. 7
- [30] Yunze Liu and Li Yi. Map: Unleashing hybrid mamba-transformer vision backbone’s potential with masked autoregressive pretraining. *arXiv preprint arXiv:2410.00871*, 2024. 3
- [31] Yue Liu, Yunjie Tian, Yuzhong Zhao, Hongtian Yu, Lingxi Xie, Yaowei Wang, Qixiang Ye, Jianbin Jiao, and Yunfan Liu. Vmamba: Visual state space model. In *Advances in Neural Information Processing Systems*, pages 103031–103063. Curran Associates, Inc., 2024. 3
- [32] Ze Liu, Yutong Lin, Yue Cao, Han Hu, Yixuan Wei, Zheng Zhang, Stephen Lin, and Baining Guo. Swin Transformer: Hierarchical vision transformer using shifted windows. In *ICCV*, pages 9992–10002. IEEE, 2021. 3
- [33] Yang Long, Gui-Song Xia, Shengyang Li, Wen Yang, Michael Ying Yang, Xiao Xiang Zhu, Liangpei Zhang, and

- Deren Li. On creating benchmark dataset for aerial image interpretation: Reviews, guidances and million-aid. *IEEE Journal of Selected Topics in Applied Earth Observations and Remote Sensing*, 14:4205–4230, 2021. 8
- [34] Cheng-Ze Lu, Xiaojie Jin, Qibin Hou, Jun Hao Liew, Ming-Ming Cheng, and Jiashi Feng. Delving deeper into data scaling in masked image modeling. *arXiv preprint arXiv:2305.15248*, 2023. 2, 6
- [35] Utkarsh Mall, Bharath Hariharan, and Kavita Bala. Change-aware sampling and contrastive learning for satellite images. In *CVPR*, pages 5261–5270, 2023. 2, 7
- [36] Oscar Mañas, Alexandre Lacoste, Xavier Giró-i-Nieto, David Vázquez, and Pau Rodríguez. Seasonal contrast: Unsupervised pre-Training from uncurated remote sensing data. In *ICCV*, pages 9394–9403. IEEE, 2021. 2, 7
- [37] Maryam Mehmood, Ahsan Shahzad, Bushra Zafar, Amsa Shabbir, and Nouman Ali. Remote sensing image classification: A comprehensive review and applications. *Mathematical problems in engineering*, 2022(1):5880959, 2022. 7
- [38] Matías Mendieta, Boran Han, Xingjian Shi, Yi Zhu, and Chen Chen. Towards geospatial foundation models via continual pretraining. In *ICCV*, pages 16806–16816, 2023. 2, 7
- [39] Dilxat Muhtar, Xueliang Zhang, Pengfeng Xiao, Zhenshi Li, and Feng Gu. Cmid: A unified self-supervised learning framework for remote sensing image understanding. *IEEE Transactions on Geoscience and Remote Sensing*, 61:1–17, 2023. 7
- [40] Vishal Nedungadi, Ankit Kariryaa, Stefan Oehmcke, Serge Belongie, Christian Igel, and Nico Lang. Mmearth: Exploring multi-modal pretext tasks for geospatial representation learning. In *ECCV*, pages 164–182. Springer, 2024. 2
- [41] Mubashir Noman, Muzammal Naseer, Hisham Cholakkal, Rao Muhammad Anwer, Salman H. Khan, and Fahad Shahbaz Khan. Rethinking transformers pre-training for multi-spectral satellite imagery. In *CVPR*, pages 27811–27819. IEEE, 2024. 1, 2, 4, 7
- [42] Nathalie Petteorelli, Henrike Schulte to Bühne, Ayesha Tulloch, Grégoire Dubois, Cate Macinnis-Ng, Ana M Queirós, David A Keith, Martin Wegmann, Franziska Schrodt, Marion Stellmes, et al. Satellite remote sensing of ecosystem functions: Opportunities, challenges and way forward. *Remote Sensing in Ecology and Conservation*, 4(2):71–93, 2018. 1
- [43] Yu Qi, Fan Yang, Yousong Zhu, Yufei Liu, Liwei Wu, Rui Zhao, and Wei Li. Exploring stochastic autoregressive image modeling for visual representation. In *AAAI*, pages 2074–2081. AAAI Press, 2023. 3
- [44] Colorado J. Reed, Ritwik Gupta, Shufan Li, Sarah Brockman, Christopher Funk, Brian Clipp, Kurt Keutzer, Salvatore Candido, Matt Uyttendaele, and Trevor Darrell. Scale-MAE: A scale-aware masked autoencoder for multiscale geospatial representation learning. In *ICCV*, pages 4065–4076. IEEE, 2023. 1, 2, 4, 7
- [45] Sucheng Ren, Xianhang Li, Haoqin Tu, Feng Wang, Fangxun Shu, Lei Zhang, Jieru Mei, Linjie Yang, Peng Wang, Heng Wang, Alan Yuille, and Cihang Xie. Autoregressive pretraining with mamba in vision. In *ICLR*, 2025. 2, 3, 4, 5, 7
- [46] Olaf Ronneberger, Philipp Fischer, and Thomas Brox. U-net: Convolutional networks for biomedical image segmentation. In *Medical image computing and computer-assisted intervention—MICCAI 2015: 18th international conference, Munich, Germany, October 5-9, 2015, proceedings, part III 18*, pages 234–241. Springer, 2015. 7
- [47] Mannat Singh, Quentin Duval, Kalyan Vasudev Alwala, Haoqi Fan, Vaibhav Aggarwal, Aaron Adcock, Armand Joulin, Piotr Dollar, Christoph Feichtenhofer, Ross Girshick, Rohit Girdhar, and Ishan Misra. The effectiveness of mae pre-pretraining for billion-scale pretraining. In *ICCV*, pages 5484–5494, 2023. 2, 6
- [48] Xian Sun, Peijin Wang, Wanxuan Lu, Zicong Zhu, Xiaonan Lu, Qibin He, Junxi Li, Xuee Rong, Zhujun Yang, Hao Chang, et al. Ringmo: A remote sensing foundation model with masked image modeling. *IEEE Transactions on Geoscience and Remote Sensing*, 2022. 7
- [49] Maofeng Tang, Andrei Cozma, Konstantinos Georgiou, and Hairong Qi. Cross-scale mae: A tale of multiscale exploitation in remote sensing. In *Proceedings of the 37th International Conference on Neural Information Processing Systems*, Red Hook, NY, USA, 2023. Curran Associates Inc. 1, 2
- [50] Keyu Tian, Yi Jiang, Zehuan Yuan, BINGYUE PENG, and Liwei Wang. Visual autoregressive modeling: Scalable image generation via next-scale prediction. In *Advances in Neural Information Processing Systems*, pages 84839–84865. Curran Associates, Inc., 2024. 2, 3, 5
- [51] Adam Van Etten, Dave Lindenbaum, and Todd M Bacastow. Spacenet: A remote sensing dataset and challenge series. *arXiv preprint arXiv:1807.01232*, 2018. 7
- [52] Di Wang, Jing Zhang, Bo Du, Gui-Song Xia, and Dacheng Tao. An empirical study of remote sensing pretraining. *IEEE Transactions on Geoscience and Remote Sensing*, 61:1–20, 2023. 2
- [53] Di Wang, Qiming Zhang, Yufei Xu, Jing Zhang, Bo Du, Dacheng Tao, and Liangpei Zhang. Advancing plain vision transformer toward remote sensing foundation model. *IEEE Transactions on Geoscience and Remote Sensing*, 61:1–15, 2023. 1, 4, 7
- [54] Di Wang, Jing Zhang, Minqiang Xu, Lin Liu, Dongsheng Wang, Erzong Gao, Chengxi Han, Haonan Guo, Bo Du, Dacheng Tao, and Liangpei Zhang. Mtp: Advancing remote sensing foundation model via multi-task pretraining. *IEEE Journal of Selected Topics in Applied Earth Observations and Remote Sensing*, pages 1–24, 2024. 7
- [55] Fengxiang Wang, Wanrong Huang, Shaowu Yang, Qi Fan, and Long Lan. Learning to learn better visual prompts. In *Proceedings of the AAAI Conference on Artificial Intelligence*, pages 5354–5363, 2024. 3
- [56] Fengxiang Wang, Hongzhen Wang, Di Wang, Zonghao Guo, Zhenyu Zhong, Long Lan, Jing Zhang, Zhiyuan Liu, and Maosong Sun. Scaling efficient masked autoencoder learning on large remote sensing dataset. *arXiv preprint arXiv:2406.11933*, 2024. 1, 4, 7
- [57] Chen Wei, Haoqi Fan, Saining Xie, Chao-Yuan Wu, Alan Yuille, and Christoph Feichtenhofer. Masked feature prediction for self-supervised visual pre-training. In *CVPR*, pages 14668–14678, 2022. 3

- [58] Curtis E Woodcock, Thomas R Loveland, Martin Herold, and Marvin E Bauer. Transitioning from change detection to monitoring with remote sensing: A paradigm shift. *Remote Sensing of Environment*, 238:111558, 2020. 1
- [59] Gui-Song Xia, Jingwen Hu, Fan Hu, Baoguang Shi, Xiang Bai, Yanfei Zhong, Liangpei Zhang, and Xiaoqiang Lu. Aid: A benchmark data set for performance evaluation of aerial scene classification. *IEEE Transactions on Geoscience and Remote Sensing*, 55(7):3965–3981, 2017. 7
- [60] Tete Xiao, Yingcheng Liu, Bolei Zhou, Yuning Jiang, and Jian Sun. Unified perceptual parsing for scene understanding. In *ECCV*, pages 418–434, 2018. 7
- [61] Zhenda Xie, Zheng Zhang, Yue Cao, Yutong Lin, Jianmin Bao, Zhuliang Yao, Qi Dai, and Han Hu. Simmim: A simple framework for masked image modeling. In *CVPR*, pages 9653–9663, 2022. 1, 3, 7
- [62] Fanglong Yao, Wanxuan Lu, Heming Yang, Liangyu Xu, Chenglong Liu, Leiye Hu, Hongfeng Yu, Nayu Liu, Chubo Deng, Deke Tang, Changshuo Chen, Jiaqi Yu, Xian Sun, and Kun Fu. Ringmo-sense: Remote sensing foundation model for spatiotemporal prediction via spatiotemporal evolution disentangling. *IEEE Trans. Geosci. Remote. Sens.*, 61:1–21, 2023. 1
- [63] Jing Yao, Danfeng Hong, Chenyu Li, and Jocelyn Chanussot. Spectralmamba: Efficient mamba for hyperspectral image classification. *arXiv preprint arXiv:2404.08489*, 2024. 2, 3
- [64] Xiaohui Yuan, Jianfang Shi, and Lichuan Gu. A review of deep learning methods for semantic segmentation of remote sensing imagery. *Expert Systems with Applications*, 169:114417, 2021. 1
- [65] Mi Zhang, Bingnan Yang, Xiangyun Hu, Jianya Gong, and Zuxun Zhang. Foundation model for generalist remote sensing intelligence: Potentials and prospects. *Science Bulletin*, 69(23):3652–3656, 2024. 5
- [66] Sijie Zhao, Hao Chen, Xueliang Zhang, Pengfeng Xiao, Lei Bai, and Wanli Ouyang. Rs-mamba for large remote sensing image dense prediction. *IEEE Transactions on Geoscience and Remote Sensing*, 62:1–14, 2024. 3
- [67] Jinghao Zhou, Chen Wei, Huiyu Wang, Wei Shen, Cihang Xie, Alan Yuille, and Tao Kong. Image bert pre-training with online tokenizer. In *ICLR*, 2021. 3
- [68] Lianghui Zhu, Bencheng Liao, Qian Zhang, Xinlong Wang, Wenyu Liu, and Xinggang Wang. Vision mamba: Efficient visual representation learning with bidirectional state space model. In *ICML*, 2024. 2, 3
- [69] Qinfeng Zhu, Yuanzhi Cai, Yuan Fang, Yihan Yang, Cheng Chen, Lei Fan, and Anh Nguyen. Samba: Semantic segmentation of remotely sensed images with state space model. *Heliyon*, 10(19):e38495, 2024. 3